Comparative Study of Mechanical and Electrical Characteristics of High-Strength and Conventional Electrical Steel for EV Traction High-Speed Multilayer IPMSM Using Rare-Earth Free PM

Ki-O Kim[1], Young-Hoon Jung[1,2], Jin-Cheol Park[1], and Myung-Seop Lim[1]

[1]Department of Automotive Engineering, Hanyang University, Seoul 04763, Republic of Korea
[2]Department of Automotive Engineering, Yeungnam University, Gyeongsan 38541, Republic of Korea

In this article, the electrical and mechanical characteristics of multilayer interior permanent magnet synchronous motors (ML-IPMSMs) using ferrite permanent magnets (PMs) are compared when driven at high speeds with respect to the type of electrical steel. In high-speed operation, the mechanical and electrical characteristics of ML-IPMSMs vary depending on the number of PM layers, PM shape, number of bridges, and bridge thickness. In addition, ferrite PMs have a lower coercive force than neodymium (Nd) PMs; therefore, irreversible demagnetization (ID) must be considered, and it is affected by the number of PM layers and PM shape of ML-IPMSMs. Thus, when designing a multilayer IPMSM using ferrite PMs for electric vehicle (EV) traction, all characteristics should be considered. Compared to conventional electrical steel (CES), high-strength electrical steel (HSES) offers advantages in mechanical properties, allowing for greater flexibility in ML shape. Consequently, it is possible to design a shape with improved electrical performance when compared to CES by adjusting the ML shape. In this article, all characteristics of each ML-IPMSM using HSES and CES are reviewed via finite element analysis (FEA), and the benefits of HSES-applied motors for high-speed driving motors are presented. To verify the validity of the review content in this article, experiments are conducted on the manufactured motor, and FEA results are compared with the test results.

Index Terms— **Conventional electrical steel (CES), ferrite permanent magnet, high-strength electrical steel (HSES), irreversible demagnetization (ID), multilayer interior permanent magnet synchronous motor (ML-IPMSM), safety factor (SF), traction motor.**

I. Introduction

ELECTRIC vehicles (EVs) have become the mainstream means of transportation, and the demand for high-performance traction electric motors is increasing. As traction motors for EVs require high power, they are becoming faster and must be designed to enable high-speed driving. An interior permanent magnet synchronous motor (IPMSM) using a neodymium (Nd) permanent magnet (PM) exhibits high power density, high efficiency, and wide speed-range operation. Hence, it is used by many vehicle manufacturers [1]. However, Nd PMs, which use rare-earth metals as raw materials, are unstable in supply due to the limited production area of rare-earth metals and have a high price and large price volatility depending on international circumstances. Therefore, various studies have been conducted on IPMSMs using Nd PM reduction or rare-earth free PMs [2], [3], [4], [5], [6]. In [5], multilayer IPMSM (ML-IPMSM) using a ferrite PM was adopted as an alternative to an IPMSM using an Nd PM for EV traction because it generates a high reluctance torque. In [5] and [6], various design methods were presented that considered the electrical and mechanical characteristics of ML-IPMSMs using ferrite PMs for traction applications. The mechanical stability of the ML-IPMSM varied depending on the number of PM layers, number of bridges, bridge thickness, and PM shape. In addition, depending on the parameters, electrical characteristics, such as back electromotive force (BEMF), torque, efficiency, and irreversible demagnetization (ID) of the PMs, also change. Therefore, motor designers should carefully consider the mechanical and electrical characteristics based on their shapes. However, in each study, the information on electrical steel is simply presented as material information on the electrical steel at the time of design. To realize high-power motors, the maximum driving speed tends to increase; accordingly, research on high-strength electrical steel (HSES) that will enable high-speed driving of motors is required. However, studies on motors using HSES are extremely rare, and no studies have compared ML-IPMSMs using ferrite PMs for EV traction with conventional electrical steel (CES). Table I lists the mechanical characteristics of the CES and HSES, and Fig. 1 shows the B–H curve and iron loss data of the two electrical steels. The CES material is 27PNX1350F, and the HSES material is 35PNT600Y. As presented in Table I, the yield stress of the HSES is approximately 1.5 times greater than that of the CES. Therefore, the magnitude of stress that the rotor can withstand during high-speed rotation can be increased when compared with the CES. Furthermore, as shown in Fig. 1, the B–H curve characteristics of the CES are superior to those of the HSES, and the iron losses per unit weight of the CES at 50 and 400 Hz are smaller than those of the HSES. Consequently, given that the two materials exhibit a mechanical and electrical trade-off relationship, the design of the ML-IPMSM varies based on the material. In this article, the mechanical and electrical characteristics of an ML-IPMSM

Manuscript received 28 March 2023; revised 1 June 2023; accepted 15 June 2023. Date of publication 19 June 2023; date of current version 24 October 2023. Corresponding author: M.-S. Lim (e-mail: myungseop@hanyang.ac.kr).

Color versions of one or more figures in this article are available at https://doi.org/10.1109/TMAG.2023.3287535.

Digital Object Identifier 10.1109/TMAG.2023.3287535

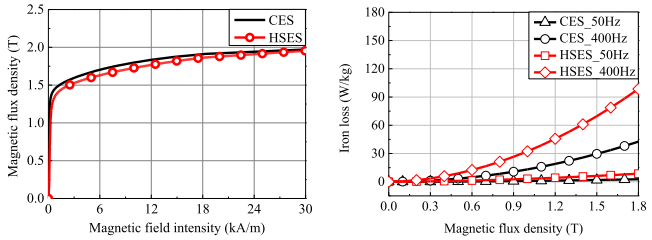

Fig. 1. Electrical characteristics of electrical steel. (a) B–H curve. (b) Iron loss.

TABLE I
COMPARISON OF ELECTRICAL STEEL MECHANICAL PROPERTIES

Contents	Unit	CES (27PNX1350F)	HSES (35PNT600Y)
Density	kg/m^3	7600	7600
Yield stress	MPa	420	620
Poisson's ratio	-	0.3	0.3
Young's modulus	GPa	180	178

TABLE II
MOTOR SPECIFICATIONS

Contents	Unit	Value	Note
Maximum power	kW	120	
Maximum torque	Nm	189	
Maximum speed	rpm	15000	
Maximum current	A_{rms}	300	
DC link voltage	V_{dc}	680	
Pole & slot number	-	8/96	
Split ratio	-	0.74	
Shape ratio	-	0.74	
Rotor core material	-	CES or HSES	
Stator core material	-	CES	
PM residual induction	T	0.392	100°C

with ferrite PM for EV traction were compared using a finite element analysis (FEA) when CES and HSES were applied.

II. DESIGN SPECIFICATION AND ANALYSIS CONDITION

The design motor specifications used in this article are summarized in Table II. In Table II, the split ratio and the shape ratio are expressed as follows:

$$\text{Split ratio} = \frac{D_r}{D_s} \tag{1}$$

$$\text{Shape ratio} = \frac{L_{stk}}{D_r} \tag{2}$$

where D_r is the outer diameter of the rotor; D_s is the outer diameter of the stator; L_{stk} is the stack length. The materials used for the rotor core are CES and HSES. To ensure a fair comparison, the stator shapes, materials, and winding specifications remain the same. The rotor design variables of the ML-IPMSM, considering the manufacturing process, are shown in Fig. 2. The first-layer PM shape is aligned with the central axis line, and a gap of 0.2 mm between the rotor core and PM is applied. Given that the shape of the PM or the thickness of the bridge is affected by manufacturability, it is necessary to select them by reflecting manufacturability when setting the design parameters. The rotor shape based on the

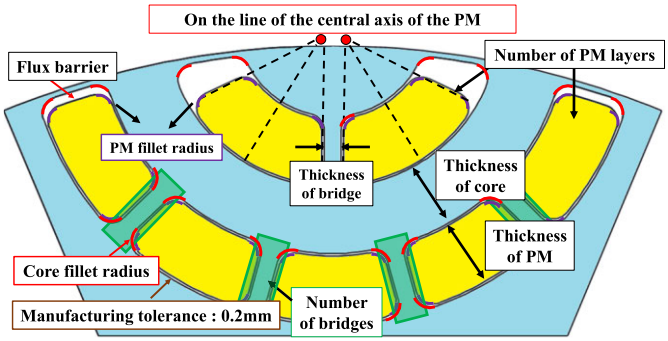

Fig. 2. Design variables of the rotor ML-IPMSM.

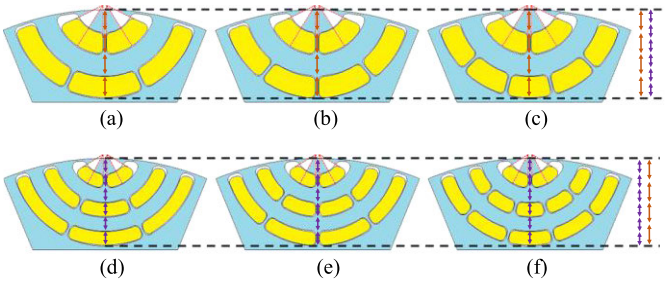

Fig. 3. Rotor shape of ML-IPMSM according to the number of layers and number of bridges. (a) Two-layer, two bridges. (b) Two-layer, three bridges. (c) Two-layer, four bridges. (d) Three-layer, two bridges. (e) Three-layer, three bridges. (f) Three-layer, four bridges.

number of PM layers and bridges is shown in Fig. 3. In Fig. 3, as the number of PM layers increased, the PM thickness decreased; however, the total sum of the PM thickness and core thickness is the same. In addition, the ratio of PM thickness and core thickness for each layer is the same. Given that the PM thickness affects the reluctance torque, the ratio that can utilize high reluctance torque was selected [5]. The number of PM layers and bridges for each rotor material were determined by considering the safety factor (SF), ID of the PM, and maximum torque. The SF can be expressed as follows:

$$\text{SF} = \frac{\sigma_{ys}}{\sigma_{max}} \tag{3}$$

where σ_{ys} is the yield stress; σ_{max} is the maximum stress applied to the rotor due to the rotation. The SF is obtained at 1.2 times the maximum speed in this article. In addition, it is assumed that the SF 1.2 or more is mechanically stable. The maximum torque is obtained under 300 A_{rms} phase current and 45° current phase angle because the ML-IPMSM has a large reluctance torque. The occurrence of ID was determined based on the minimum residual magnetic flux density (MRMFD) of the PM operating point via FEA. Given that the coercive force of the ferrite PM decreases as the temperature decreases, the analysis was performed by applying 1.2 times the maximum current based on −40 °C. Fig. 4 shows the demagnetization curve at −40 °C of ferrite PM used in this article. The permeance coefficient varies depending on the shape of the motor. Hence the operating point of the PM can be formed at a point higher or lower than the knee point according to the shape of the motor. When the magnetic flux density at the operating point is below 0.05 T, ID is considered to have

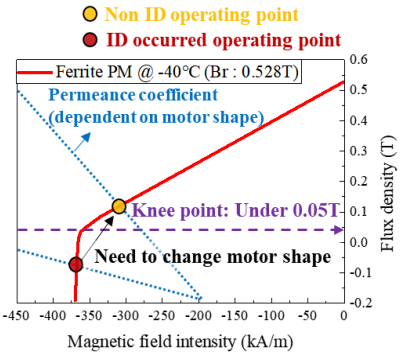

Fig. 4. Demagnetization curve of ferrite PM.

TABLE III
NUMBER OF BRIDGES AND BRIDGE THICKNESS WITH RESPECT TO THE NUMBER OF PM LAYERS

Number of layers	Number of bridges	Bridge thickness (mm)
2	2	0.6 ~ 1.8 mm 0.3mm step
	3	
	4	
3	2	
	3	
	4	

occurred. Although MRMFD can confirm the occurrence of ID, it is difficult to compare the effects of demagnetization for each model. Therefore, the demagnetization ratio (DR) was calculated and compared for each model. The DR can be expressed as follows:

$$\text{DR}\ (\%) = \frac{\lambda_{\text{ph,demag}} - \lambda_{\text{ph,noload}}}{\lambda_{\text{ph,noload}}} \times 100 \tag{4}$$

where $\lambda_{\text{ph,demag}}$ is the peak value of the no-load phase linkage flux after the demagnetization analysis, and $\lambda_{\text{ph,noload}}$ is the peak value of the no-load phase linkage flux before demagnetization analysis. In this article, it was determined that ID occurs when the DR is greater than 1%.

III. COMPARISON OF MECHANICAL AND ELECTRICAL CHARACTERISTICS WITH RESPECT TO ELECTRICAL STEEL

A. Number of PM Layers and Bridges

Table III lists the number of bridges and thickness value of bridge with respect to the number of PM layers. The ratio of the PM thickness to the core thickness was maintained as same, and other variables were held constant. The SF, torque, and DR for different rotor materials are shown in Fig. 5. As shown in Fig. 5(a) and (b), the SF increases as the number of PM layers, bridges, and bridge thickness increase for the CES and HSES rotors. However, when the number of layers was three, the DR increased significantly compared with when the number of PM layers was two, and the torque tended to decrease. Therefore, considering SF, DR, and torque, the numbers of PM layers and bridges were set to two and four, respectively.

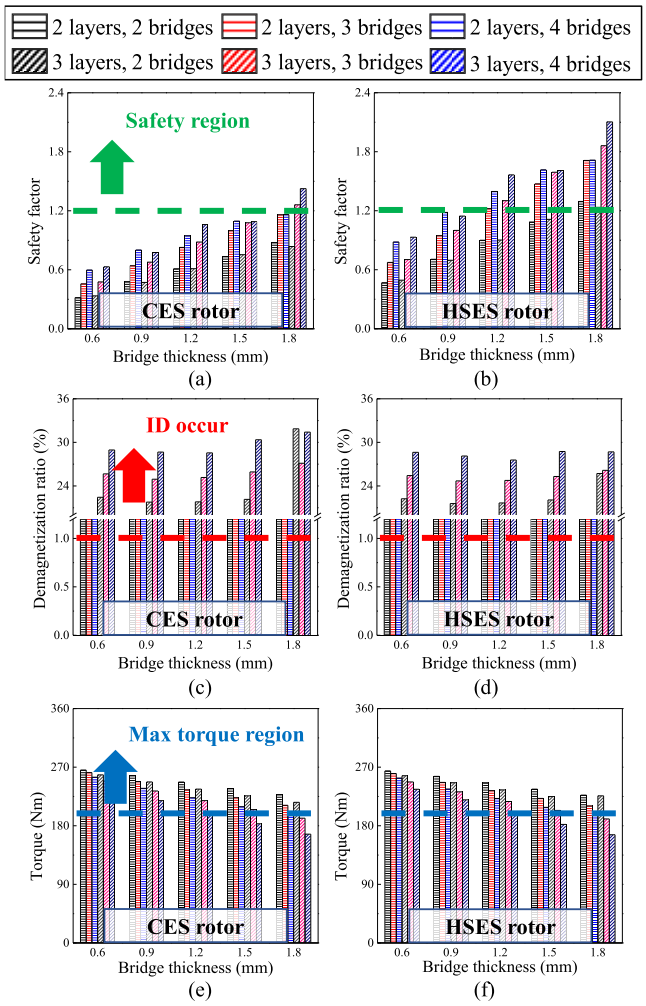

Fig. 5. Mechanical and electrical characteristics according to rotor material, the number of layers, the number of bridges, and bridge thickness. (a) SF of CES. (b) SF of HSES. (c) DR of CES. (d) DR of HSES. (e) Torque of CES. (f) Torque of HSES.

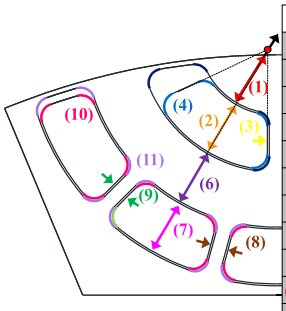

No.	Design variables	1 level	2 level	3 level
(1)	1st layer core thickness	3.2	3.7	4.2
(2)	1st layer PM thickness	8	8.5	9
(3)	1st layer bridge thickness	0.6	1.2	1.8
(4)	1st layer PM fillet radius	1.0	1.25	1.5
(5)	1st layer core fillet radius	1.0	1.25	1.5
(6)	2nd layer core thickness	3.0	3.5	4
(7)	2nd layer PM thickness	8	8.5	9
(8)	2nd layer center bridge thickness	0.6	1.2	1.8
(9)	2nd layer side bridge thickness	0.6	1.2	1.8
(10)	2nd layer PM fillet radius	1.0	1.5	2.0
(11)	2nd layer core fillet radius	1.0	1.5	2.0

Fig. 6. Design variables for the ANOVA.

B. Design Variables for the Analysis of Variance

To be used as an ML-IPMSM for traction, the mechanical SF must be satisfied, and ID must be avoided because ferrite PMs are used. Given that there is a trade-off relationship between mechanical and electrical performance, it is necessary to check the effect of the rotor design variables on performance. Design variables that significantly contributed to the SF, DR, and torque were determined using analysis of variance

TABLE IV
BOUNDARIES OF DESIGN VARIABLES

Design variables	notation	Unit	Min	Max
1st layer core thickness	x_1	mm	3.2	5.0
1st layer PM thickness	x_2	mm	8.0	9.0
1st layer bridge thickness	x_3	mm	0.6	1.8
2nd layer core thickness	x_4	mm	3.0	4.0
2nd layer PM thickness	x_5	mm	8.0	9.0
2nd layer center bridge thickness	x_6	mm	0.6	1.8
2nd layer side bridge thickness	x_7	mm	0.6	1.8
2nd layer PM fillet radius	x_8	mm	1.0	2.0

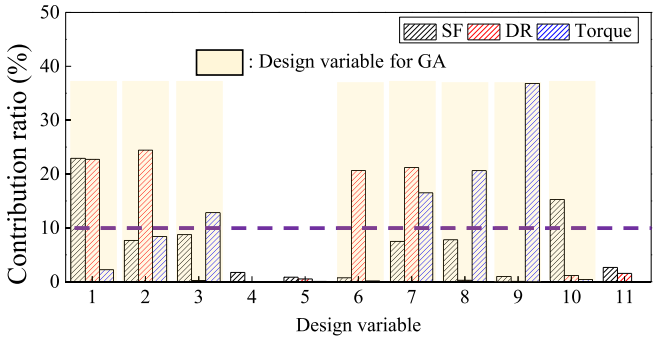

Fig. 7. Contribution ratio according to design variables for each performance.

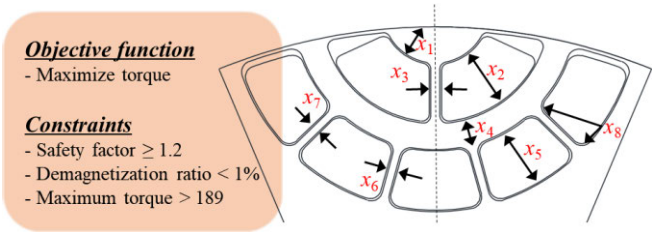

Fig. 8. Objective function, design constraints, and shape of design variables.

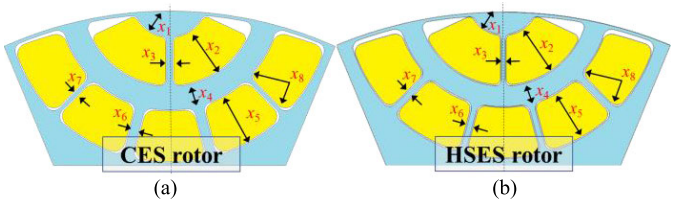

(a) (b)

Fig. 9. Optimization result shapes for each model. (a) CES (b) HSES.

(ANOVA). The design variables for ANOVA are shown in Fig. 6. Each design variable was reviewed at 3 levels within the manufacturing feasible range. As shown in Fig. 7, for the main design variables, only those with a contribution ratio of 10% or more for each performance are selected. Design variable numbers 4, 5, and 11 with contributions less than 10% are determined by the trends of the main effects plot of SF, DR, and torque. Accordingly, 1.0, 1.25, and 1.5 mm were selected in order.

C. Comparison of Optimal Results of CES and HSES Models

To determine the variables satisfying the SF, DR, and torque criteria, a genetic algorithm (GA) based on the Kriging surrogate model is used. The objective functions, design constraints,

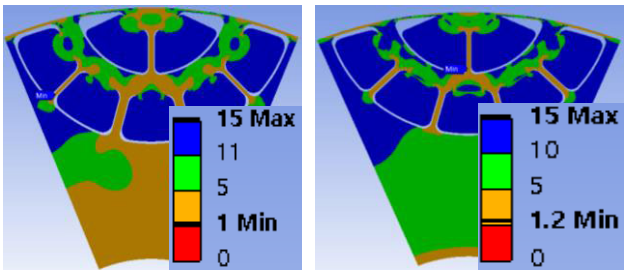

(a) (b)

Fig. 10. SF distribution for each optimal design model. (a) CES. (b) HSES.

TABLE V
OPTIMAL RESULTS FOR EACH MODEL

Design variables	notation	Unit	CES	HSES
1st layer core thickness	x_1	mm	4.0	3.2
1st layer PM thickness	x_2	mm	8.3	8.5
1st layer bridge thickness	x_3	mm	1.0	0.6
2nd layer core thickness	x_4	mm	4.0	3.1
2nd layer PM thickness	x_5	mm	8.7	8.6
2nd layer center bridge thickness	x_6	mm	1.6	0.9
2nd layer side bridge thickness	x_7	mm	0.6	1.0
2nd layer PM fillet radius	x_8	mm	1.9	1.6

and the shape of design variables are shown in Fig. 8. Table IV summarizes the maximum and minimum values of the design variables. The optimization results using GA are shown in Fig. 9 and Table V. In the CES model, it was not possible to find an optimal result with the SF of 1.2 or more and the DR 1% or less, as shown in Fig. 8. Hence, the result at SF limit 1 or higher was shown. As shown in Fig. 9 and Table V, in the case of the CES rotor, the thickness of the bridge is relatively larger than that of the HSES rotor to increase mechanical stability. Figs. 10 and 11 show the mechanical and electrical characteristics of CES and HSES models, respectively. Although the thickness of the bridge is thinner in the HSES model than that in the CES model, the SF is higher. Therefore, HSES model exhibits better mechanical stability. In addition, the leakage flux is small due to the thin bridge, therefore, the BEMF is higher than CES model, and the efficiency is relatively higher throughout the driving range. The average torque within the current limit at the base speed for each model achieved 189 Nm, and the torque ripple of the two models was 5.86% and 6.03%, respectively. Also, at the maximum speed of 50 Nm, the torque ripple is 4.40% and 5.32%, respectively. As seen in those values of the torque ripple, the torque ripple of the two models is almost the same. In both optimal results for each rotor material, DR is 0.2, and as shown in Fig. 11(c) and (d), MRMFD is greater than 0.05 T. Hence, The ID does not occur. Test verification is limited to the HSES model, as the HSES model has significantly better mechanical and electrical performance than the CES model.

IV. VERIFICATION

An ML-IPMSM with ferrite PM machines using HSES rotor was prototyped for design validation. Fig. 12 shows the fabricated rotor, stator, inverter, and test setup. Fig. 13 shows the FEA and test results for the 1000 r/min no-load

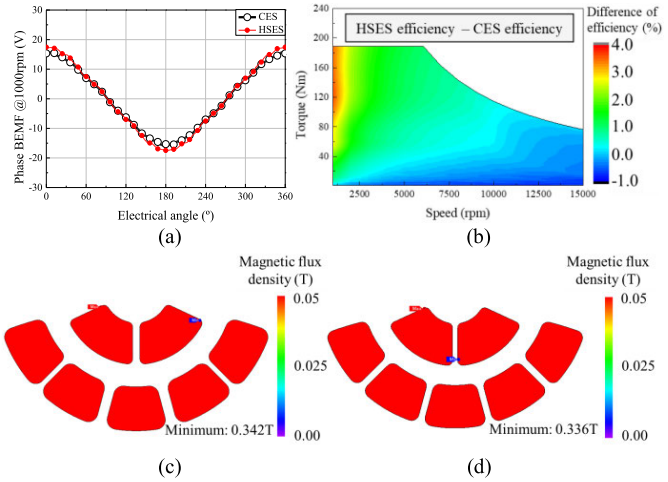

Fig. 11. Comparision of electrical characteristics for each optimal design model. (a) BEMF. (b) Difference of efficiency map. (c) Demagnetization of CES. (d) Demagnetization of HSES.

TABLE VI
LOAD TEST AND FEA COMPARISON RESULTS

Speed (rpm)	Load (Arms / beta)	Content	Torque (Nm)	Error (%)	Eff. (%)	Error (%)
5500	283.9 / 48.7	FEA	189.0	1.25	89.5	-0.78
		Exp.	191.4		90.2	
7500	224.4 / 47.7	FEA	146.9	-1.38	92.6	0.22
		Exp.	144.9		92.8	
15000	122.2 / 66.4	FEA	50.9	-0.79	90.0	2.81
		Exp.	50.5		92.6	

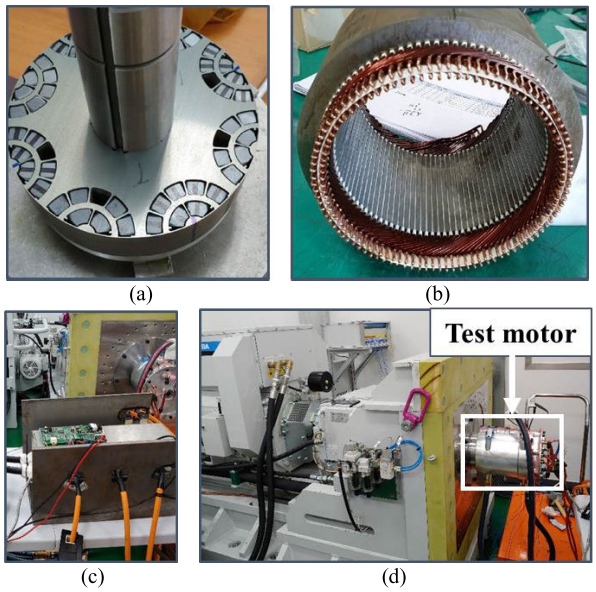

Fig. 12. Experimental system. (a) Rotor. (b) Stator. (c) Inverter. (d) Test setup.

condition. As shown in Fig. 13, the FEA and test results of line-to-line BEMF are 23.03 and 22.63 V_{rms}, respectively, and the error between the two results is 1.77%. Table VI lists the load data comparing the test and FEA results. The load test points were tested at maximum torque load, high power load, and maximum speed load, respectively. The input current conditions of the load test were the same as those calculated for the FEA. At all test points, the torque error between the

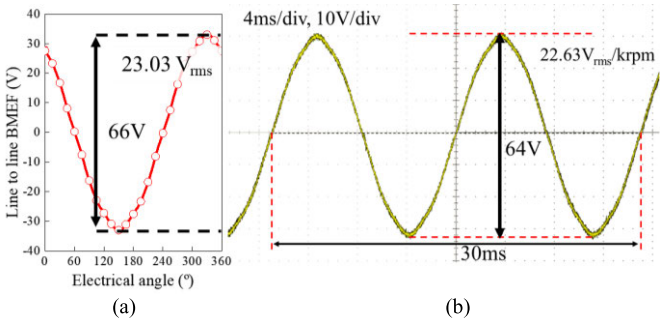

Fig. 13. No-load line to line BEMF. (a) FEA. (b) Experiment.

test and FEA results was less than 2%, and the efficiency error was less than 3%. From these test results, the FEA result of the HSES model is reliable. Hence, it can be seen that the comparison of the characteristics of CES and HSES was also well analyzed. In addition, the mechanical stability at high speeds was verified by performing a load test at the maximum speed.

V. CONCLUSION

In this article, a comparison of performance changes is presented with respect to the rotor material of an ML-IPMSM using a ferrite PM and design method. Although HSES has inferior electrical performance compared to CES, when designing the ML-IPMSM considering SF, ID, and torque, the overall performance of the motor with an HSES rotor is superior to that of a motor with a CES rotor, owing to the advantage of mechanical properties. The HSES model was fabricated and tested under specific load conditions. The FEA torque and efficiency were verified using the load test results with an error within 2% and 3%, respectively. In addition, as the load test was performed at the maximum rotational speed, mechanical stability at the maximum speed was verified. Therefore, the performance comparison results of the ML-IPMSM for each rotor material and proposed design method can be considered valid.

REFERENCES

[1] E. Sayed, R. Yang, J. Liang, M. H. Bakr, B. Bilgin, and A. Emadi, "Design of unskewed interior permanent magnet traction motor with asymmetric flux barriers and shifted magnets for electric vehicles," *Electr. Power Compon. Syst.*, vol. 48, nos. 6–7, pp. 652–666, Sep. 2020.

[2] K. Sone, M. Takemoto, S. Ogasawara, K. Takezaki, and H. Akiyama, "A ferrite PM in-wheel motor without rare earth materials for electric city commuters," *IEEE Trans. Magn.*, vol. 48, no. 11, pp. 2961–2964, Nov. 2012.

[3] C. Yunyun, C. Tongle, Z. Xiaoyong, and D. Yu, "Optimization of a new asymmetric-hybrid-PM machine with high torque density and low torque ripple considering the difference of magnetic materials," *IEEE Trans. Magn.*, vol. 58, no. 2, pp. 1–5, Feb. 2022.

[4] M. Park, J. Jung, D. Kim, J. Hong, and M. Lim, "Design of high torque density multi-core concentrated flux-type synchronous motors considering vibration characteristics," *IEEE Trans. Ind. Appl.*, vol. 55, no. 2, pp. 1351–1359, Mar./Apr. 2019.

[5] Y. Jung, M. Park, K. Kim, J. Chin, J. Hong, and M. Lim, "Design of high-speed multilayer IPMSM using ferrite PM for EV traction considering mechanical and electrical characteristics," *IEEE Trans. Ind. Appl.*, vol. 57, no. 1, pp. 327–339, Jan./Feb. 2021.

[6] E. Sayed et al., "Design of multilayer concentric ferrite-magnet machines for a traction application," *IEEE Trans. Transport. Electrific.*, vol. 7, no. 3, pp. 1548–1560, Sep. 2021.